INTERNATIONAL JOURNAL OF AUTOMOTIVE AND MECHANICAL ENGINEERING
ISSN: 2229-8649 e-ISSN: 2180-1606
VOL. 21, ISSUE 3, 2024, 11652 – 11662
DOI: https://doi.org/10.15282/ijame.21.3.2024.16.0899

RESEARCH ARTICLE

Numerical Study on Single and Multi-Element NACA 43018 Wing Airfoil with Leading-Edge Slat and Slotted Flap

Setyo Hariyadi S.P.[1,4]*, Bambang Juni Pitoyo[1], Nyaris Pambudiyatno[2], Sutardi[3], Wawan Aries Widodo[3]

[1]Aircraft Maintenance Engineering Department, Politeknik Penerbangan Surabaya, Jemur Andayani I/73 Wonocolo, Surabaya, 60236, Indonesia

[2]Air Navigation Engineering Department, Politeknik Penerbangan Surabaya, Jemur Andayani I/73 Wonocolo, Surabaya, 60236, Indonesia

[3]Mechanical Engineering Department, Faculty of Industrial Technology and Systems Engineering, Institut Teknologi Sepuluh Nopember, Jalan Arif Rahman Hakim, Sukolilo, Surabaya, 60111, Indonesia

[4]Aircraft Operation Training Division, Akademi Penerbang Indonesia Banyuwangi, Jl. Pantai Blimbingsari, Dusun Krajan, Blimbingsari, Rogojampi, Banyuwangi Regency, East Java 68462 Indonesia

ABSTRACT - An optimal wing configuration is crucial for achieving the best performance during various flight phases, including take-off, cruising, and landing. Such configurations also contribute to maximizing the aircraft's cruising range. This study compares the aerodynamic performance of NACA 43018 wings under different conditions: without high-lift devices, with a slotted flap, and with a combination of a leading-edge slat and slotted flap. Numerical simulations were conducted using the k-ε Realizable turbulence model at twelve different angles of attack, with a flow speed of 120 m/s. The results demonstrate that multiple-element wings significantly improve aerodynamic performance, particularly at low angles of attack, by reducing the induced drag coefficient and delaying flow separation.

ARTICLE HISTORY
Received : 06th Feb. 2024
Revised : 08th Aug. 2024
Accepted : 02nd Sept. 2024
Published : 20th Sept. 2024

KEYWORDS
NACA 43018
Multiple element wing
Slotted flap
Leading-edge slat
Aerodynamic performance

1. INTRODUCTION

Aircraft designers are constantly striving to improve the aerodynamic performance of aircraft as much as possible. One of the desired goals is fuel efficiency by increasing lift as much as possible and reducing drag as much as possible [1]. To achieve this, commercial aircraft almost always use high-lift devices on their wings. The goal is clearly to increase the lifting force as much as possible. Various types of high-lift devices have been developed by aircraft designers to suit the companies that produce them. Therefore, it is difficult to categorize the types of high-lift devices into specific types and characteristics. Existing high-lift devices on commercial aircraft include flaps, vortex generators, leading edge slats (slat slots), winglets, fences, and others. Various references categorize these high-lift devices into various things. Some include high lift devices, primary control surfaces, secondary control surfaces, and so on. However, the primary effect of using these devices is to increase lift, although some, such as flaps, also influence other aspects of aircraft movement [2]. Therefore, high-lift devices are always present on various types of aircraft of various sizes and distances. Each high-lift device configuration has different effects on various aspects of the aircraft. It can be single-element or multi-element. Each condition and configuration composition have different results, especially in different airfoil or wing types and different circumstances. This is interesting because each position will produce different effects, so it is necessary to predict the effects of these conditions using simulations and experiments.

Several experts have examined the performance of leading-edge slats in several configurations, including Chen et al. [3], dos Santos et al. [4], Kuntumala et al. [5], Singh et al.[6], and Antoniou et al.[7]. Some researchers also provide special conditions, for example, due to icing, as in the studies of Raffaele et al. [8] and Xu et al. [9]. Similar conditions are also carried out in bird strike conditions Elumalai et al. [10]. In addition, some researchers have focused on multiple-element wings, which are a combination of several high-lift devices, especially leading-edge slats and flaps. The researchers who focused on multiple-element wings, especially the cove effect of leading slats, include Wang et al.[11], Yu and Mi [12], and Markesteijn et al. [13]. Researchers focusing on multiple-element wings, especially the noise effect of leading slats, include Sanders et al. [14] and Wei et al. [15]. Jiangsheng Wang et al. [11] investigated the impact of the Reynolds number on the shear layer interaction of a multi-element wing airfoil (30P30N) using TR-PIV and hydrogen bubble imaging. In an open subsonic wind tunnel, the Reynolds number (Rec), which ranges from 9.3×10^3 to 3.05×10^4, was employed. The critical Rec range, which is new for the low Reynolds number flow in the multi-element plane, is discovered to be 1.27×10^4 to 1.38×10^4 based on the fluctuation of the dominating flow structure. Based on this important interval, there are two sorts of slat wakes. At the tip of the shear layer, rolling doesn't happen if R_{ec} is smaller than this crucial interval. When Rec is greater than this critical range, rolling occurs at the shear layer at the upper range, similar to the case at high Reynolds numbers. This rolling and evolution lead to the simultaneous presence of spanwise and streamwise vortices.

***CORRESPONDING AUTHOR | Setyo Hariyadi S.P.** | ✉ setyo_hariyadi@poltekbangsby.ac.id

Lance W. Traub et al. [16] studied the application of leading-edge slats at low Reynolds numbers. Oil flow visualization was used to conduct the investigation at R_e = 250,000 in a wind tunnel. The leading-edge gap size at various angles of attack was the variation that was employed. The findings indicate that while large gap sizes may be taken into consideration to boost lift, minor slat extensions negatively impact aerodynamic performance. Even if the lift increases greatly, the usage of leading-edge slats must make up for the increased drag as a penalty. Hariyadi et al. [17] examined the use of a multi-element wing airfoil NACA 43018 in the form of a leading-edge slat combined with a plain flap. The conditions used are flap deflection 0°, 15°, and 30° at a freestream velocity of 432 km/h. The research was conducted using numerical simulation for take-off, cruising, and landing conditions. An increase in induced drag coefficient was observed for all configurations when compared to the plain wing. The lift increase becomes less significant as the total drag coefficient increases significantly. The increase in induced drag coefficient can be seen from the formation of tip vortex in the area behind the wing where the addition of leading-edge combined with flap deflection of 30° produces the widest area compared to other configurations. The configuration of the multi-element wing has been studied by experts, especially on the configuration of each component. Certain configurations will be used in certain flight phases as well. Research similar to this article, for example in Hongyan et al. [18], who used a configuration between leading-edge slat and flap. Hongyan et al. focused on the aerodynamic performance of the DLR F11 wing of the German Aerospace Center regarding lift, drag, and moment coefficient. However, research on phase-of-flight configurations and comparisons of single and multi-element wings is still rare to find in journals. What exists is to compare the configuration among the multiple-element itself, for example, in the research of Hariyadi et al. [17] and [19], and that too using plain flaps.

This study compares the aerodynamic performance of plain wing and leading edge and leading-edge slat equipped with slotted flaps. The condition used is during cruising, with 0° flap deflection, when the NACA 43018 wing airfoil is used on ATR 72-500 and 600 aircraft series, while the freestream velocity is 120 m/s. Research on the ATR 72 500 and 600 aircraft series is important because it is used in various areas around the world, especially Indonesia, which connects various islands, especially Eastern Indonesia. Currently, ATR 72 500 and 600 series aircraft only use flaps as high-lift devices without leading-edge slats. This article presents an alternative to using a combination of leading-edge slats and flaps and compares it to using only flaps. The aerodynamic performance displayed is lift, drag, and lift-to-drag ratio. In addition, the visualization of the pressure coefficient and vorticity magnitude around the midspan is used to show the effect of the single and multiple-element wings.

2. METHODS AND MATERIALS

2.1 Mathematical Model

The forces on the wing of an aircraft, according to Filippone [20], include:

$$D = \frac{1}{2} C_D \rho A V_\infty^2 \tag{1}$$

$$L = \frac{1}{2} C_L \rho A V_\infty^2 \tag{2}$$

In conditions of increasing speed, the onset of boundary layers, and steady-state conditions, the lift and drag coefficients depend on changes in several variables, including:

$$C_L = C_L(M, \alpha) \tag{3}$$

$$C_D = C_D(M, \alpha) \tag{4}$$

From the theory of aerodynamics, the following is obtained:

$$C_L = C_{L0} + C_{L\alpha}(\alpha - \alpha_0) \tag{5}$$

$$C_{L\alpha} = \frac{2\pi}{1 + \frac{2}{AR}}(\alpha - \alpha_0) \tag{6}$$

$$C_D = C_{D0} + \eta C_{L\alpha} \alpha^2 \tag{7}$$

At subsonic speed, a common drag equation is

$$C_D = C_{D0} + k C_L^2 \tag{8}$$

$$k = \frac{1}{e\pi AR} \tag{9}$$

Glide factor or aerodynamic efficiency for subsonic speed becomes:

$$\frac{L}{D} = \frac{C_L}{C_D} = \frac{C_L}{C_{D0} + k C_L^2} \tag{10}$$

The glide ratio at transonic and supersonic speed can be expressed as:

$$\frac{L}{D} = \frac{C_L}{C_D} = \frac{C_{L\alpha}\alpha}{C_{D0} + \eta C_{L\alpha}\alpha^2} = \frac{1}{\frac{C_{D0}}{C_{L\alpha}\alpha} + \eta\alpha} \tag{11}$$

2.2 Numerical Simulation

This research uses numerical simulation in Ansys 19.1. continuing the research of Hariyadi et al.[17], [19], [21]. Numerical simulations using the turbulent model the k-ε Realizable according to the research of Mulvany et al. [22], where the turbulent model is considered better than other turbulent models in the Ansys application for cases like this. The freestream velocity used is 120 m/s or Re = 3.76 x10^5. The angles of attack used include: 0º, 2º, 4º, 6º, 8º, 10º,12º,15º, 16º,17º,19º and 20º. With the selection of the angle of attack, a good aerodynamic performance graph is expected so that the position of the angle of attack where the stall occurs is known more efficiently. However, the use of numerical simulation in this study is slightly different from that of Tobing, S [23], who used the same parameters but at different Re. The wing used is straight so that the analysis produced with the delta shape used high Re as research Jamei S. et al. [24], Kasim, K.A. et al. [25], Madan I. et al. [26], and Said M. et al. [27]. The simulation domain in this study refers to Mulvany et al.[22] with an extension of the area behind the wing as far as five times the chordline to be able to show the vorticity magnitude that occurs by the research of Hariyadi et al. [19], [21], [28]. Figure 1 shows the simulation domain of this study. The extension of the area behind the wing aims to show the effect of vorticity on the wing more clearly, both in length and strength. Figure 2 shows the configuration of the research model used in this study.

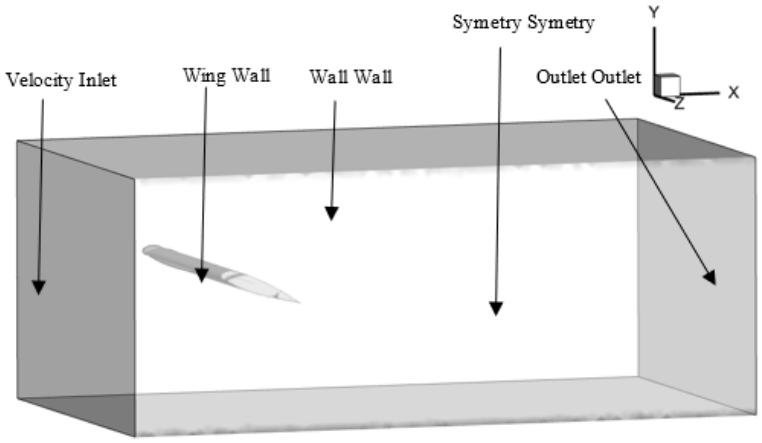

Figure 1. Simulation domain

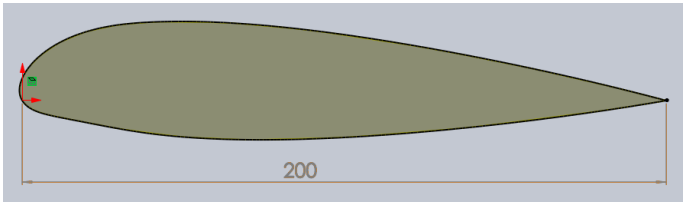

Plain wing

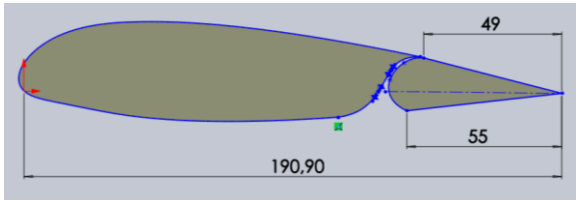

Plain wing with slotted flap

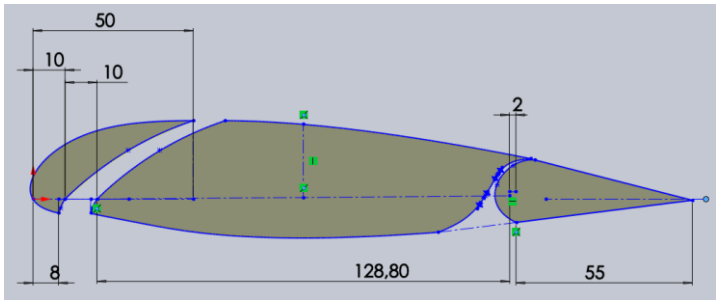

Plain wing with LE slat and slotted flap

Figure 2. Research model

2.3 Grid Independency

The use of numerical simulations with grid independence as a validation criterion is an attempt to make the results obtained match reality. Aircraft using NACA 43018 wing airfoils and similar aircraft use a cruising speed of about 120

m/s which can be achieved due to the use of turbine engines. The use of grid independence as validation has been used in several other studies, for example, in the research of Urbano et al. [29] and Dinh et al. [30], although using different test models and parameters.

Table 1. Grid independency of the three-dimensional wing airfoil NACA 43018 [21], [28]

Number of *Mesh*	Number of Nodes	C_D	y^+	Skewness Average
Mesh A	862642	0,297	0,257	0,311
Mesh B	832000	0,216	0,176	0,314
Mesh C	706906	0,19	0,145	0,328
Mesh D	639000	0,15	0,11	0,343
Mesh E	504086	0,08	0,04	0,336

Table 1 shows the grid independency of the lime mesh plain wing airfoil NACA 43018. According to the research of Anderson [31] and Mulvany et al. [22], the difference in C_D produced by each mesh is no more than 2% from that produced by the other mesh quantities. This is to show the consistency of the results of the selected mesh so that the difference is not too large. In addition, to get the best results, a smaller y+ is required, which is less than one, according to the research of Kontogiannis et al. [32], [33] and Roy et al.[34] as well as a skewness average of less than 0.35, as research by Hariyadi et al. [35]. Based on these criteria, Mesh B was selected for the next stage of research.

3. SIMULATION RESULTS

3.1 Aerodynamic Performance

The overall drag coefficient of the three study configurations, the slotted flap, the plain wing, and the slotted flap with the leading-edge slat, is displayed in Figure 3. The plain wing structure yields the highest total drag coefficient when compared to other configurations, as shown in Figure 3(a). A slotted flap with a leading-edge slat and slotted flap comes in second. The variables included friction, pressure, and induced drag coefficients that add up to the overall drag coefficient are depicted in the following picture. In contrast to the overall drag coefficient data, the friction drag coefficient in Figure 3(b) displays a small value and a relatively minor difference across all research setups. The plain wing structure exhibits a modest decrease in value at an angle of attack of $\alpha = 15^o$ but increases at subsequent angles of attack. These data are displayed at all angles of attack.

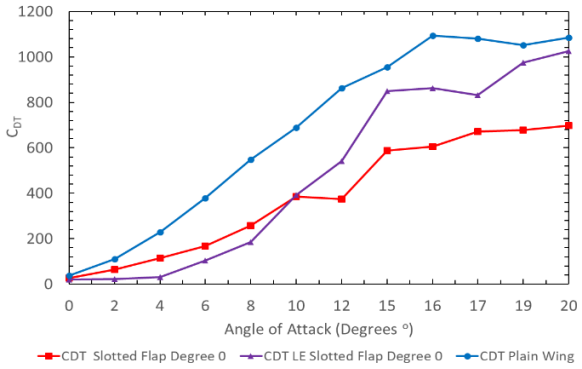

(a) Total drag coefficient

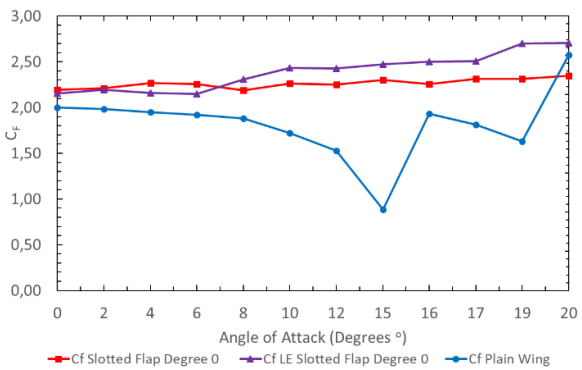

(b) Friction drag coefficient

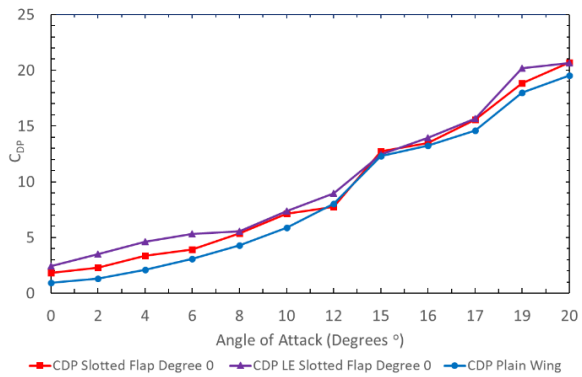

(c) Pressure drag coefficient

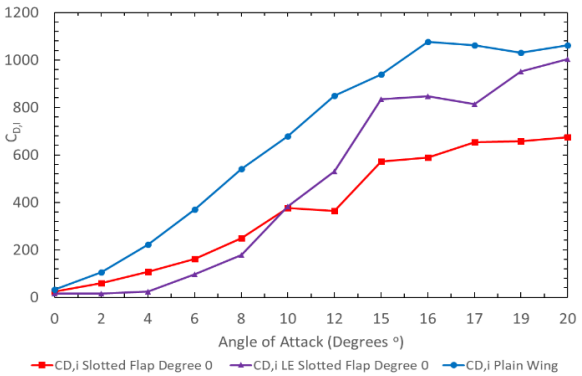

(d) Induced drag coefficient

Figure 3. Drag coefficient results from the study

The pressure drag coefficient values for each research arrangement are displayed in Figure 3(c). The values of the three configurations grow with increasing angle of attack and do not differ significantly. The slotted flap configuration with a leading-edge slat exhibits a little greater value than the other configurations despite the modest change in value. The induced drag coefficient of the study is displayed in Figure 3(d) for all angles of attack of the research configurations. At all angles of attack, the plain wing configuration exhibits the highest value in comparison to the other forms. Compared to the slotted flap design alone, the slotted flap configuration with a leading-edge slat demonstrated a greater induced drag coefficient value following the angle of attack ($\alpha = 10^o$).

The lift coefficient for each research setup is displayed in Figure 4(a). When compared to the other forms, the plain wing configuration has the highest lift coefficient value. The arrangement stalls at an attack angle of $\alpha = 16^o$. In the alternative arrangements, the slotted flap came to a stop at an angle of attack of $\alpha = 10^o$, whereas the slotted flap, including a leading-edge slat, came to a stop at an angle of attack of $\alpha = 15^o$, following an extremely swift rise in the lift coefficient value. The lift-to-drag ratio for each study setup is displayed in Figure 4(b). It is evident from Figure 4(b) that the impact of deploying high lift devices at angles of attack greater than $\alpha = 10^o$ is not significantly different. It is evident that the slotted flap configuration with a leading-edge slat has the highest value among the other configurations for the angles of attack below $\alpha = 10^o$. The lift-to-drag ratio is not significantly different between the slotted flap and plain wing types.

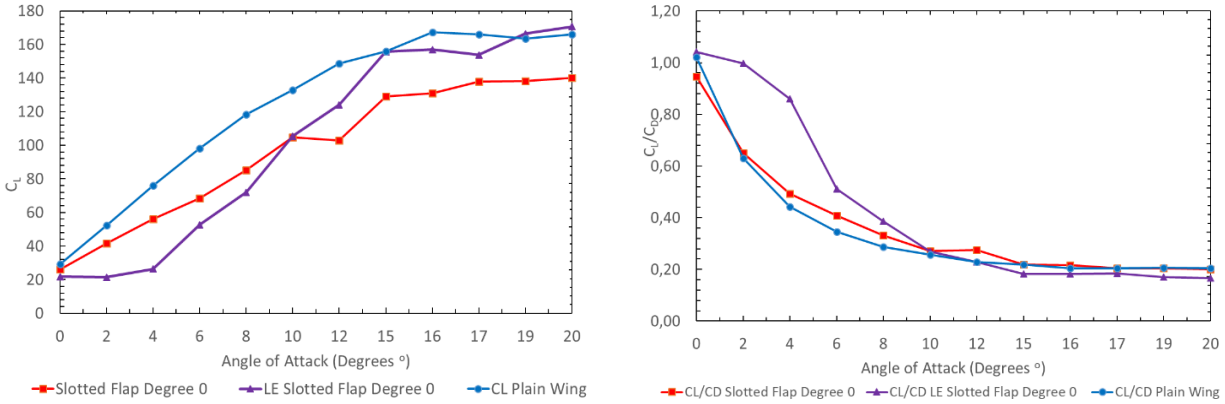

(a) Lift coefficient (b) Lift to drag ratio

Figure 4. Lift coefficient and lift to drag ratio results from the research

3.2 Pressure Coefficient Contour Visualization

The pressure coefficient contours for all configurations at angles of attack $\alpha = 0^o$, 6^o, and 16^o are visualized in Figure 5. It is evident that the contour changes start to shift from the leading edge towards the trailing edge in the slotted flap design with a leading-edge slat at $\alpha = 0^o$ (Figure 5(a)). This contour shift is still more extensive than the slotted flap's, though. While still very slight, the color gradation changes in the slotted flap configuration (Figure 5(b)) are more frequent than in the slotted flap configuration with a leading-edge slat (Figure 5(c)). This demonstrates how the inclusion of high-lift devices and the space between the primary airfoil body act as a differentiator. It is easier to see the difference in color gradation at the angle of attack $\alpha = 6^o$.

At the angle of attack $\alpha = 6^o$, the tip vortex's function in the wingtip region is shown. The downwash marks are wider in the plain wing arrangement (Figure 5(d)) than they are in the other configurations. At an angle of attack of $\alpha = 6^o$, the slotted flap with the addition of the leading-edge slat (Figure 5(f)) exhibits the smallest downwash markings in comparison to the other configurations, highlighting the significance of the gap between the primary airfoil body and the inclusion of high lift devices. This is not the case with the slotted flap (Figure 5(e)), where there are more variations in the pressure coefficient value and a somewhat bigger area of the downwash markings.

Pressure coefficient contours with low values have emerged at the leading edge in all study setups at the angle of attack $\alpha = 16^o$. In all three arrangements, the area of the pressure coefficient value is found to be nearly the same. On the other hand, the leading-edge slat-equipped slotted flap (Figure 5(i)) exhibits a more varied value change in the vicinity of the leading-edge slat gap. Additionally, Figure 5 demonstrates that the slotted flap (Figure 5(g)) and the slotted flap with the leading-edge slat (Figure 5(h)) separate with a minor delay. The plain wing's green tint, which is closer to the leading edge than the other versions, indicates this. The area near the wingtips requires care as well. When compared to the slotted flap configuration with a leading-edge slat, the plain wing and slotted flap configurations exhibit a significant fluctuation in their shapes, indicating the influence of downwash in this area. Though the value limit is smaller than for the other two designs, the extent of the downwash effect on the slotted flap with a leading-edge slat has a broader area.

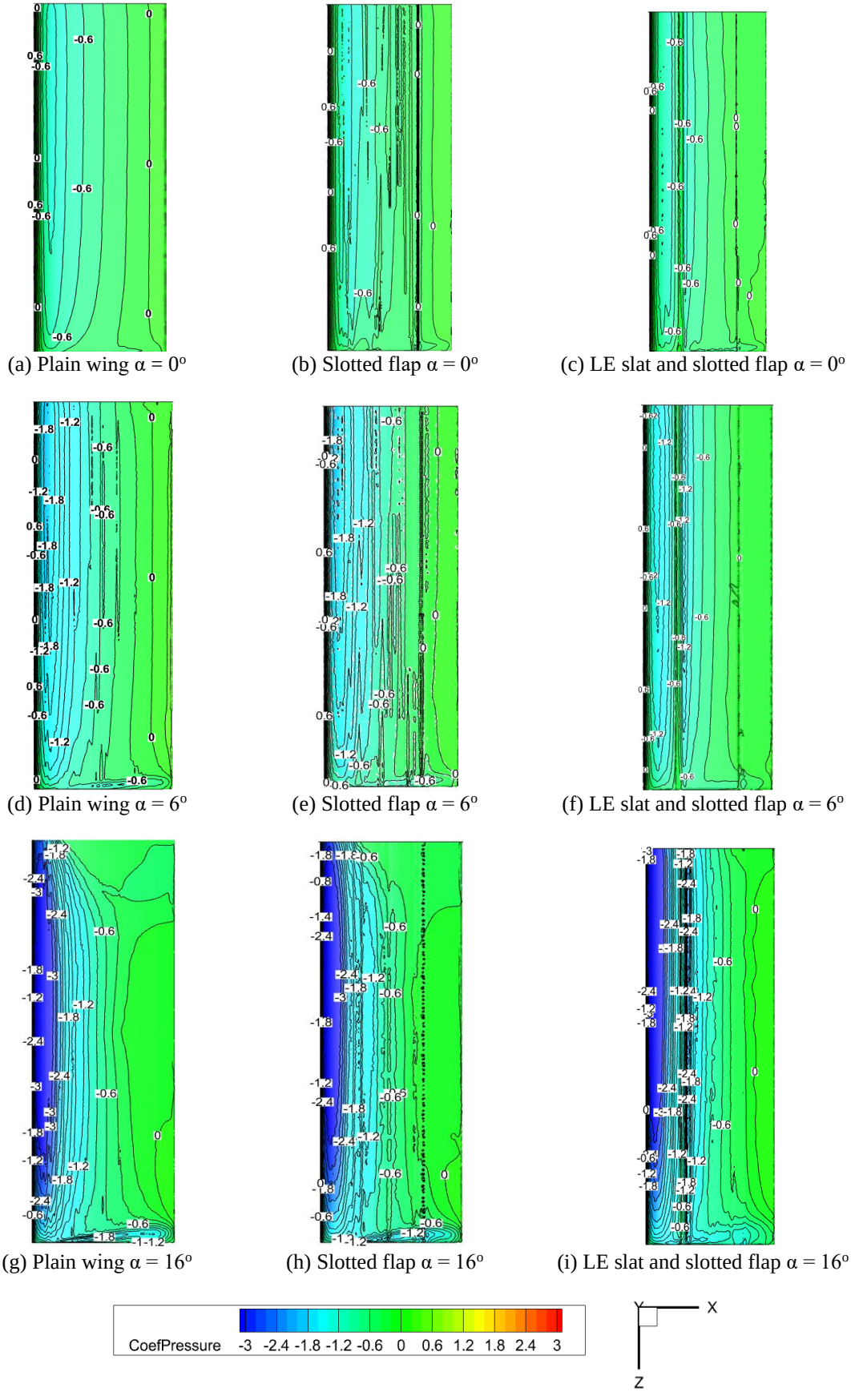

(a) Plain wing α = 0º (b) Slotted flap α = 0º (c) LE slat and slotted flap α = 0º

(d) Plain wing α = 6º (e) Slotted flap α = 6º (f) LE slat and slotted flap α = 6º

(g) Plain wing α = 16º (h) Slotted flap α = 16º (i) LE slat and slotted flap α = 16º

Figure 5. Pressure coefficient visualization of all configuration

3.3 Vorticity Magnitude

Figure 6 shows the vorticity magnitude on the x-y axis for all study configurations. In the plain wing configuration (Figure 6(a)), it can be seen that the vorticity magnitude has the longest length compared to the other configurations, especially on the midspan side. Slotted flaps equipped with leading-edge slats (Figure 6(c)) have vorticity magnitudes that are also long, especially in the area approaching the wingroot side, although not as long as the plain wing configuration. The slotted flap configuration (Figure 6(b)) shows the shortest vorticity magnitude compared to the other configurations both at the midspan and the area approaching the wingtip and wingroot.

Vorticity magnitude along the x-axis shows that the use of slotted flaps can reduce vorticity magnitude along the x-axis compared to plain wings. The use of leading-edge slats combined with slotted flaps reduces the vorticity magnitude even slightly. Note that this observation is only in the area around the midspan to compare how strong the effects of the leading-edge slat and slotted flap are. Observations in the wingtip area, of course, will produce a different visualization because it is strongly influenced by the formation of the downwash and tip vortex. Likewise, in the wingroot area, the formation of vorticity magnitude will be influenced by the wall, which in this case represents the fuselage of the aircraft, which will have the effect of creating a boundary layer in the area that extends towards the midspan.

The interesting thing is the value of the visualization of the vorticity magnitude contour along the x-axis with the slotted flap configuration, which has the shortest length, but the value is almost the same as the slotted flap equipped with a leading-edge slat. Additional data must be provided regarding how much vorticity is generated, as shown in Figure 7. Figure 7 shows the visualization of vorticity magnitude in the z-axis for all configurations. On the midspan side of the plain wing configuration (Figure 7(a)), the vorticity just behind the wing formed two pieces that have a larger area than the other side of the span. On the wingtip side, the tip vortex formed has a fairly wide area with a fairly high vorticity value. In the slotted flap configuration (Figure 7(b)), the vorticity formed just behind the wing shows an increase in area compared to the plain wing, although with almost the same value. At the wingtip, the tip vortex generated by the slotted flap configuration produces a slightly smaller area and lower value than the plain wing. In the slotted flap configuration equipped with a leading-edge slat (Figure 7(c)), the vorticity formed behind the wing is more than the vorticity formed behind the plain wing, and some also show a wider area. At the wingtip area, the tip vortex formed by the slotted flap configuration equipped with a leading-edge slat shows a wider area as well, although the resulting value is lower than the plain wing.

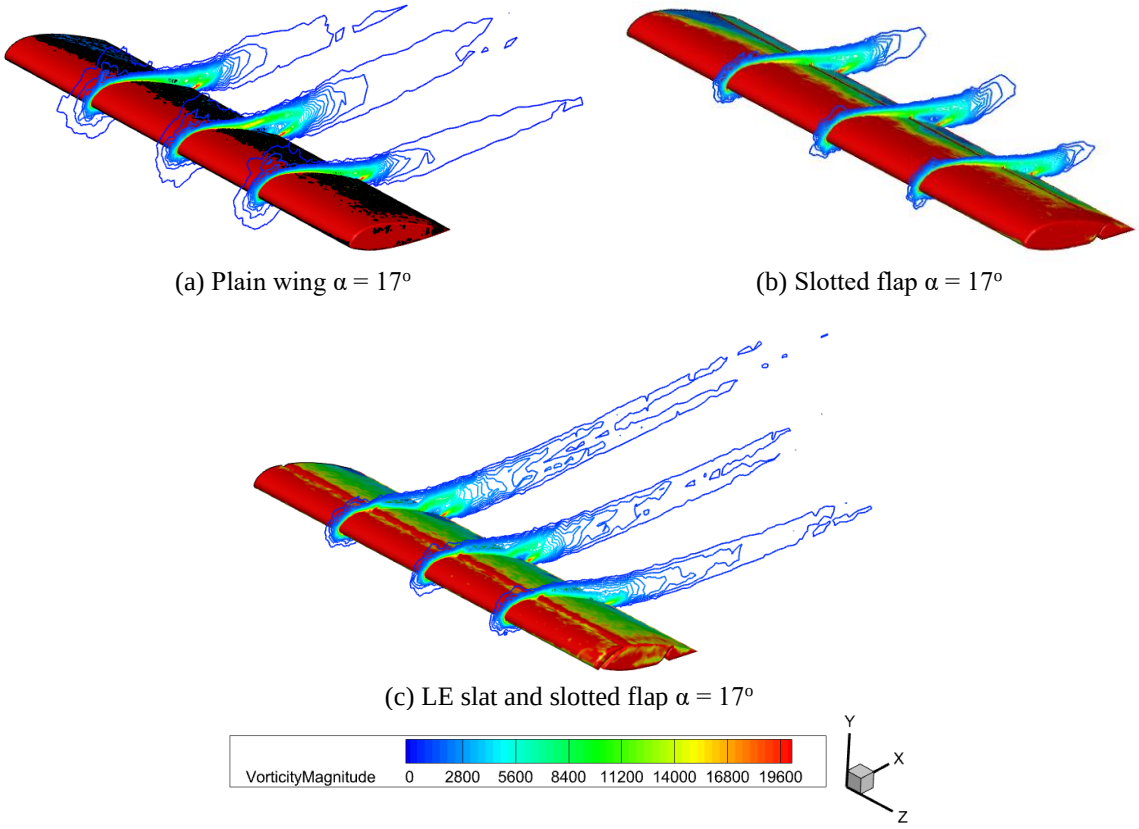

(a) Plain wing α = 17º

(b) Slotted flap α = 17º

(c) LE slat and slotted flap α = 17º

Figure 6. Visualization of Vorticity Magnitude on the x-axis for all configurations

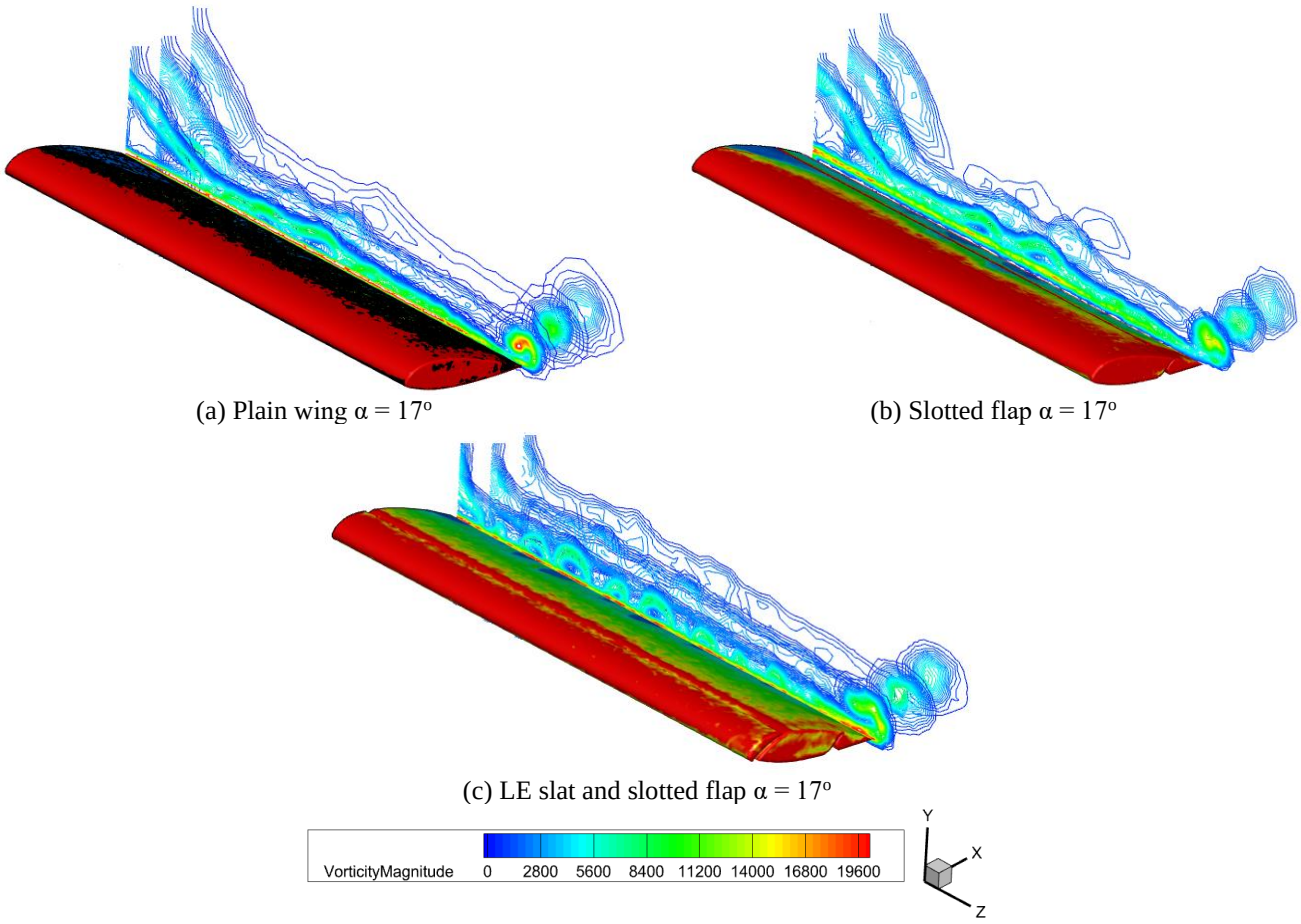

(a) Plain wing α = 17º

(b) Slotted flap α = 17º

(c) LE slat and slotted flap α = 17º

Figure 7. Visualization of Vorticity Magnitude on the z-axis for all configurations

4. DISCUSSION

According to research by Hariyadi et al. [17], [19], [36], the aerodynamic performance graph demonstrates how much the induced drag coefficient contributes to the production of the overall drag coefficient. The plain wing's lift creation, which yields the maximum value, has a high induced drag coefficient effect. As a result, the lift-to-drag ratio decreases up to the attack angle of α = 15º. The pressure coefficient contour visualization indicates that the separation at the trailing edge area will be slightly delayed due to the space between the main wing and the flap. The model with slotted flaps exhibits modest fluctuations in color values, but the plain wing displays uniformity in the trailing edge area. It is evident that separation takes place in the trailing edge area when uniform values start to appear. The leading-edge slat's presence in the vicinity of the leading edge increases the pressure variations in the top side region, where the area behind the leading-edge slat grows. The wingtip area is unaffected by the slotted flap's installation, as evidenced by the barely noticeable variation in the downwash mark form between the slotted flap configuration and the plain wing. On the other hand, the leading-edge slat's existence modifies the downwash markings' shape in the region behind it, resulting in a decrease in the magnitude of the pressure contour fluctuations and a fainter color concentration.

The use of pressure coefficient contour and other contour types, such as skin friction magnitude, in numerical simulations can adequately show the evolution of fluid flow movement on the upper surface. Experimental research can also be done using oil flow visualization using Ti02 mixed with palm oil. This has been confirmed by the research of Dayanti et al. [37]. However, the effectiveness of research for high speeds, such as aircraft speeds for cruising conditions, needs to be confirmed again with experimental research, considering that the speeds used have a high range of differences. In the vorticity magnitude contours parallel to the x-axis, vorticity occurs just behind the wing in all models. This is a good thing about the NACA 43018 airfoil because there is no vorticity in the x-axis as in the studies of Fujita and Lima [38] and Hojaji et al. [39]. In Fujita and Lima's study, vorticity was formed at several positions above the upper surface in both the flat plate and airfoil models. However, the vorticity x generated by the slotted flap configuration equipped with a leading-edge slat had the longest contour compared to the other models. The shortest vorticity x length occurs in the slotted flap configuration where the same size has a smaller value.

In the vorticity magnitude contours parallel to the z-axis, the effect of using slotted flaps and leading-edge slats causes vorticity at several positions. This is an increase in the amount of vorticity compared to the study by Werner et al. [40], which had only two positions above the upper surface on a delta-shaped wing. However, the plain wing configuration has higher vorticity values at the wing tip than the others. This tip vortex supports the aerodynamic performance analysis,

showing that the plain wing produces the highest induced drag compared to other configurations, consistent with the findings of Pertiwi et al. [41].

5. CONCLUSIONS

Twelve angles of attack were used to conduct numerical simulations on three distinct configurations of the NACA 43018 airfoil wing model. The best aerodynamic performance is not usually achieved by using high-lift devices. Although it can also result in high drag, installing more high-lift devices on the wing does not guarantee that it will create the most lift. The greatest lift and drag coefficients are produced by the plain wing model, with the induced drag coefficient accounting for the majority of the drag value. According to the results of the lift-to-drag ratio, the slotted flap arrangement with a leading-edge slat has the best aerodynamic performance at low angles of attack, but at high angles of attack, it performs worse than other models.

The pressure coefficient contour visualization validates the aerodynamic performance data, wherein the plain wing's induced drag coefficient exhibits the largest tip vortex in comparison to other variants. High-lift devices, particularly the slotted flap variant with the cutting-edge slat, help to mitigate downwash on the wingtip side indirectly. Furthermore, compared to the plain wing model, the pressure variations produced by slotted flaps and leading-edge slats are much more variable, which generally lessens the possibility of separation on the upper surface. In the contours of vorticity magnitude, it is shown that the use of high-lift devices creates a wider vorticity and tends to be stronger than the plain wing. The use of a single-element wing tends to produce larger vorticity, while the use of a multiple-element wing gives rise to new vorticities compared to other models. The vorticity area behind the wingtip shows a stronger and wider vorticity area in the slotted flap model equipped with a leading-edge slat when compared to other configurations.

This research can be continued with the addition of other high-lift devices so that it will bring up completely new conditions compared to this research, which can serve as a baseline. Additional high-lift devices that can be used include vortex generators and winglets, as well as changing the type of flaps such as Fowler flaps. In addition, the wing shape can be changed to a delta shape or given an adequate swept-back angle.

REFERENCES

[1] N.N. Gavrilović, B.P. Rašuo, G.S. Dulikravich, and V.B. Parezanović, "Commercial aircraft performance improvement using winglets," *FME Transactions*, vol. 43, no. 1, pp. 1–8, 2015.

[2] S. Gudmundsson, *General Aviation Aircraft Design : Applied Methods*, First edit. New York: Butterworth-Heinemann is an imprint of Elsevier, 2013.

[3] Y.H. Chen, J.J. Miau, Y.P. Chen, and Y.R. Chen, "Blunt leading-edge effect on spanwise-varying leading-edge contours of an UCAV configuration," *Journal of Fluid Science and Technology*, vol. 18, no. 1, pp. 1–11, 2023.

[4] F.L. dos Santos, K. Venner, and L.D. de Santana, "Turbulence distortion effects for leading-edge noise prediction," *28th International Congress on Sound and Vibration, ICSV 2022*, pp. 1–8, 2022.

[5] G. Kuntumalla, Y. Meng, M. Rajagopal, R. Toro, H. Zhao, HC. Chang et al., "Joining techniques for novel metal polymer hybrid heat exchangers," *ASME International Mechanical Engineering Congress and Exposition*, vol. 59384, p. V02BT02A018, 2019.

[6] P. Singh, L. Neuhaus, O. Huxdorf, J. Riemenschneider, J. Wild, J. Peinke, and M. Hölling, "Experimental investigation of an active slat for airfoil load alleviation," *Journal of Renewable and Sustainable Energy*, vol. 13, no. 4, p. 043304, 2021.

[7] S. Antoniou, S. Kapsalis, P. Panagiotou, and K. Yakinthos, "Parametric investigation of leading-edge slats on a blended-wing-body UAV using the Taguchi method," *Aerospace*, vol. 10, no. 8, p. 720, 2023.

[8] D. Raffaele, T.P. Waters, E. Rustighi, and U. Kingdom, "Wave propagation in an aircraft wing slat for de-icing purposes," *3rd Euro-Mediterranean Conference on Structural Dynamics and Vibroacoustics. Università degli Studi di Napoli*, pp. 17–20, 2020.

[9] X. Xu, T. Wang, Y. Fu, Y. Zhang, and G. Chen, "Numerical research of an ice accretion delay method by the bio-inspired leading edge," *Aerospace*, vol. 9, no. 12, p. 774, 2022.

[10] E.S. Elumalai, A.G. Agarwal, B.K. Singh and G. Krishnaveni, "Numerical simulation of bird strike effect on a composite wing leading edge," *Test Engineering and Management*, vol. 83, pp. 7472–7481, 2020.

[11] J. Wang, J. Wang, and K.C. Kim, "Wake/shear layer interaction for low-Reynolds-number flow over multi-element airfoil," *Experiments in Fluids*, vol. 60, pp. 1-24, 2019.

[12] J. Yu and B. Mi, "A new flow control method of slat-grid channel-coupled configuration on high-lift device," *Applied Sciences*, vol. 13, no. 6, p. 3488 2023.

[13] A.P. Markesteijn, H.K. Jawahar, S.A. Karabasov, and M. Azarpeyvand, "GPU CABARET Solutions for 30P30N three-element high-lift airfoil with slat modification," in *2021 AIAA AVIATION Forum and Exposition*, American Institute of Aeronautics and Astronautics, p. 2115, 2021.

[14] M.P.J. Sanders, L.D. de Santana, and C.H. Venner, "The sweep angle effect on slat noise characteristics of the 30p30n high-lift model in an open-jet wind tunnel," *AIAA Aviation 2020 Forum*, p. 2557, 2020.

[15] R. Wei, Y. Liu, X. Li, and H. Zhang, "Experimental study on the oscillation of the shear layer of the slat cavity for 30P30N multi-element high-lift airfoil," *AIAA AVIATION 2023 Forum*, p. 4482, 2023.

[16] L.W. Traub and M.P. Kaula, "Effect of leading-edge slats at low Reynolds numbers," *Aerospace*, vol. 3, no. 4, p. 39, 2016.

[17] S.P. Setyo Hariyadi, B. Junipitoyo, N. Pambudiyatno, Sutardi, and W.A. Widodo, "Aerodynamic characteristics of fluid flow on multiple-element wing airfoil Naca 43018 with leading-edge slat and plain flap," *Journal of Engineering Science and Technology*, vol. 18, no. 1, pp. 36–50, 2023.

[18] H. Lv, X. Zhang, and J. Kuang, "Numerical simulation of aerodynamic characteristics of multi-element wing with variable flap," *Journal of Physics: Conference Series*, vol. 916, no. 1, p. 012005, 2017.

[19] S.P.S. Hariyadi, N. Pambudiyatno, Sutardi, and P.F. Dyan, "Aerodynamic characteristics of the wing airfoil NACA 43018 in take off conditions with slat clearance and flap deflection," in *Recent Advances in Mechanical Engineering: Select Proceedings of ICOME 2021. Singapore: Springer Nature Singapore*, pp. 220–229, 2022.

[20] A. Filippone, *Flight Performance of Fixed and Rotary Wing Aircraft*, First Edit. Burlington, MA: Elsevier Ltd., 2006.

[21] S.H.S. Putro, S. Sutardi, W.A. Widodo, N. Pambudiyatno, and I. Sonhaji, "Effect of leading-edge gap size on multiple-element wing NACA 43018," *International Review of Aerospace Engineering*, vol. 15, no. 12, pp. 30–40, 2022.

[22] N.J. Mulvany, L. Chen, J.Y. Tu, and B. Anderson, "Steady-state evaluation of two-equation RANS (Reynolds-Averaged Navier-Stokes) turbulence models for high-Reynolds number hydrodynamic flow simulations," Department of Defence, Australian Government, DSTO Platform Sciences Laboratory, Australia, 2004.

[23] S. Tobing, "Lift generation of an elliptical airfoil at a Reynolds number of 1000," *International Journal of Automotive and Mechanical Engineering*, vol. 16, no. 2, pp. 6738–6752, 2019.

[24] S. Jamei, A. Maimun, N. Azwadi, M.M. Tofa, S. Mansor, and A. Priyanto, "Ground viscous effect on 3D flow structure of a compound wing-in-ground effect," *International Journal of Automotive and Mechanical Engineering*, vol. 9, pp. 1550–1563, 2014.

[25] K.A. Kasim, P. Segard, S. Mat, S. Mansor, M.N. Dahalan, N.A.R.N. Mohd et al., "Effects of the propeller advance ratio on delta wing UAV leading edge vortex," *International Journal of Automotive and Mechanical Engineering*, vol. 16, no. 3, pp. 6958–6970, 2019.

[26] I. Madan, N. Tajudin, M. Said, S. Mat, N. Othman, M.A. Wahid et al., "Influence of active flow control on blunt-edged VFE-2 delta wing model," *International Journal of Automotive and Mechanical Engineering*, vol. 18, no. 1, pp. 8411–8422, 2021.

[27] M. Said, M. Imai, S. Mat, M.N. Dahalan, S. Mansor, M.N.M. Nasir et al., "Tuft flow visualisation on UTM-LST VFE-2 delta wing model configuration at high angle of attacks," *International Journal of Automotive and Mechanical Engineering*, vol. 17, no. 3, pp. 8214–8223, 2020.

[28] S. Hariyadi Suranto Putro, B. Junipitoyo, N. Pambudiyatno, Sutardi, and W. Aries Widodo, "Aerodynamic characteristics of fluid flow on multiple-element wing airfoil NACA 43018 with leading-edge slat and plain flap," *Journal of Engineering Science and Technology*, vol. 1, no. 1, pp. 36–50, 2023.

[29] D.G. Urbano, G. Noventa, A. Ghidoni, and A.M. Lezzi, "A semi-empirical fluid dynamic model of a vacuum microgripper based on CFD analysis," *Applied Sciences*, vol. 11, no. 16, p. 7482, 2021.

[30] V.S. Dinh, C.T. Dinh, and V.S. Pham, "Numerical study on aerodynamic characteristics of the grid fins with different grid patterns," *Physics of Fluids*, vol. 35, no. 12, p. 123117, 2023.

[31] J.D. Anderson Jr, *Computational Fluid Dynamics The Basics with Applications*. New York: McGraw-Hill, Inc, 1995.

[32] S.G. Kontogiannis and J.A. Ekaterinaris, "Design, performance evaluation and optimization of a UAV," *Aerospace Science and Technology*, vol. 29, no. 1, pp. 339–350, 2013.

[33] S.G. Kontogiannis, D.E. Mazarakos, and V. Kostopoulos, "ATLAS IV wing aerodynamic design: From conceptual approach to detailed optimization," *Aerospace Science and Technology*, vol. 56, pp. 135–147, 2016.

[34] A. Roy, A.K. Mallik, and T.P. Sarma, "A study of model separation flow behavior at high angles of attack aerodynamics," *Journal of Applied and Computational Mechanics*, vol. 4, no. 4, pp. 318–330, 2018.

[35] S.P. Setyo Hariyadi, Sutardi, W.A. Widodo, and M.A. Mustaghfirin, "Aerodynamics analysis of the wingtip fence effect on UAV wing," *International Review of Mechanical Engineering*, vol. 12, no. 10, pp. 837–846, 2018.

[36] S.S.P. Hariyadi, B. Junipitoyo, W.A. Widodo, I. Sonhaji and F.D. Pertiwi, "Numerical simulation using slats, slots, and flaps in steady flight conditions," *Advances in Science and Technology*, vol. 112, pp. 22–31, 2022.

[37] Z.T. Dayanti, S. Hariyadi, and I.S. Rifdian, "Experimental study of fluid flow characteristics in wing airfoil NACA 43018 with parabolic vortex generator using oil flow visualization," in *Proceedings of the International Conference on Advance Transportation, Engineering, and Applied Science (ICATEAS 2022)*, Surabaya: Atlantis Press International BV, pp. 52–69, 2023.

[38] Y. Fujita and M. Iima, "Aerodynamic performance of dragonfly wing model that starts impulsively: how vortex motion works," *Journal of Fluid Science and Technology*, vol. 18, no. 1, p. JFST0013, 2023.

[39] M. Hojaji, M.R. Soufivand, and R. Lavimi, "An experimental comparison between wing root and wingtip corrugation patterns of dragonfly wing at ultra-low Reynolds number and high angles of attack," *Journal of Applied and Computational Mechanics*, vol. 8, no. 4, pp. 1176–1185, 2022.

[40] M. Werner, M. Rein, K. Richter, and S. Weiss, "Experimental and numerical analysis of the aerodynamics and vortex interactions on multi-swept delta wings," *CEAS Aeronautical Journal*, vol. 14, no. 4, pp. 927–938, 2023.

[41] F.D. Pertiwi, A. Wahjudi, W.A. Widodo, and S.P. Hariyadi, "The effect of slat clearance and flap on the aerodynamic performance of the NACA 43018 wing in the landing process," in *AIP Conference Proceedings*, vol. 2677, no. 1, p. 10, 2023.

NOMENCLATURE

C	Chord line
b	Wing span
y^+	Normalized y by inner variables, $y^+ \equiv yU_\tau/v$
c_d	Profile drag coefficient
C_{DT}	Drag total coefficient, including drag pressure, drag viscous, and induced drag coefficient
D_f	Drag friction
D_p	Drag pressure
e	Oswald efficiency factor for straight-wing aircraft
ρ	Fluid density
$C_{L\alpha} = \frac{dC_{L\alpha}}{d\alpha}$	= zero-angle of attack lift coefficient
η	An induced drag coefficient
e	Factor variable between 0.74 and 0.88 (Oswald factor), which depends on the spanwise load distribution
α	The angle of attack, deg.
δ_f	The deflection angle of the flap
AR	Aspect Ratio
S	Wing planform area
V_∞	Freestream Velocity
D_i	Drag induced
C_L	Lift coefficient
LE	Leading Edge
A	Area
C_{D0}	The zero-lift drag coefficient (profile drag)
k	Induced drag factor